Title
The Topographic Design of River Channels for Form-Process Linkages

Journal
Environmental Management, 57(4)

ISSN
0364-152X 1432-1009

Authors
Brown, Rocko A
Pasternack, Gregory B
Lin, Tin

Publication Date
2015-12-26

DOI
10.1007/s00267-015-0648-0

Peer reviewed

The topographic design of river channels for form-process linkages

Rocko A. Brown[1,2]*, Gregory B. Pasternack[1], and Tin Lin[1]

University of California, Davis, One Shields Avenue, Davis, CA 95616, USA.

Environmental Science Associates. 2600 Capitol Avenue, Suite 200
Sacramento, CA 95816

* Corresponding author. Tel.: +1 510-333-5131; E-mail: rokbrown@ucdavis.edu.

Cite as: Brown, R. A., Pasternack, G. B., Lin, T. 2015. The topographic design of river channels for form-process linkages for river restoration. Environmental Management, 57 (4): 929-942. doi: 10.1007/s00267-015-0648-0

Abstract

Scientists and engineers design river topography for a wide variety of uses, such as experimentation, site remediation, dam mitigation, flood management, and river restoration. A recent advancement has been the notion of topographical design to yield specific fluvial mechanisms in conjunction with natural or environmental flow releases. For example, the flow convergence routing mechanism, whereby shear stress and spatially convergent flow migrate or jump from the topographic high (riffle) to the low point (pool) from low to high discharge, is thought to be a key process able to maintain undular relief in gravel bedded rivers. This paper develops an approach to creating riffle-pool topography with a form-process linkage to the flow convergence routing mechanism using an adjustable, quasi equilibrium synthetic channel model. The link from form to process is made through conceptualizing form-process relationships for riffle-pool couplets into geomorphic covariance structures (GCSs) that are then quantitatively embedded in a synthetic channel model. Herein, GCSs were used to parameterize a geometric model to create five straight, synthetic river channels with varying combinations of bed and width undulations. Shear stress and flow direction predictions from 2D hydrodynamic modeling were used to determine if scenarios recreated aspects of the flow convergence routing mechanism. Results show that the creation of riffle-pool couplets that experience flow convergence in straight channels require GCSs with covarying bed and width undulations in their topography as supported in the literature. This shows that GCSs are a useful way to translate conceptualizations of form-process linkages into quantitative models of channel form.

Keywords: river restoration design; riffle-pool; channel topography: flow convergence routing; synthetic rivers

1. Introduction

Scientists and engineers design river channel topography for a wide variety of uses, such as experimentation (Brown et al., 2014), irrigation (Lacey, 1929), navigation (Bhowmik et al., 1986), recreation, flood and sediment management (Chang and Osmolski, 1988), and river restoration (Pasternack, 2013). For example, in lowland gravel bed rivers riffle-pool (RP) units are often created, enhanced or restored through topographic manipulation to provide increased hydraulic and sedimentary diversity (Brown and Pasternack, 2008), enhance hyporheic exchange (Becker et al., 2013) and to create mesohabitat units needed for aquatic organisms (Elkins et al., 2007). The prescription of topographic and structural forms is often needed, since many rivers subject to restoration do not have sufficient flow, sediment, or even space, to carry out the geomorphic work necessary to passively restore key process-form linkages (Brown and Pasternack, 2008; Kondolf, 2013). For process based design of RP units it is essential that mechanisms related to their maintenance be incorporated, so that created forms are functional beyond their initial construction (Wheaton et al., 2004; Pasternack, 2013).

There have been a plethora of conceptual models used to explain riffle and pool maintenance ranging from sedimentary mechanisms (Clifford, 1993; Hodge et al., 2012; Milan 2013), hydraulic and hydrodynamic effects from variable channel geometry responsible for sediment transport patterns (Keller, 1971; Wilkinson et al. 2004;

Macwilliams et al. 2006), and more recently effects from turbulence (Thompson, 2004,2007; Marquis and Roy, 2011; MacVicar and Best, 2013). Most studies of riffle-pool maintenance rely on dual-stage width and depth variability between the riffle and pool that control hydrodynamic spatial patterns of velocity, shear stress, or Shields stress, that in turn control sediment transport patterns (Thompson et al., 1999; MacWilliams et al., 2006; Harrison and Keller, 2007; Caamano et al., 2010; Thompson, 2010). One such mechanism is spatial "flow convergence routing", the stage-dependent funneling of flow energy and momentum from riffles to pools with increasing discharge, as mediated by variations in flow width and bed elevation (MacWilliams et al., 2006; Thompson, 2010). As shown by MacWilliams et al. (2006) flow convergence routing is also thought to be encompassing of other theories of RP maintenance such as velocity reversals (Keller, 1971) and shear stress reversals or phasing (Wilkinson et al., 2004). It is important to note that a velocity reversal or convergence may not be needed to occur for pool maintenance if sediment is not routed into pools (Milan et al., 2013) or if the bed-material grain size is sufficiently different between riffles and pools (Milne, 1982; Jackson et al., 2015). Flow convergence is important to include in river restoration designs, because it has been linked to the maintenance of undular bed relief in gravel bed rivers despite large floods (White et al., 2010; Sawyer et al., 2010).

While many studies have begun to note the need for fluvial geomorphologic principles associated with RP maintenance in river design, the generation of actual design topographies is often not discussed nor how they can be translated to other locations (Wheaton et al., 2004; Rhoads et al., 2011; Schwartz et al., 2014). A new approach to prescriptively generating design topography is to use the synthetic river valley (SRV) framework of Brown et al. (2014). The SRV framework uses a geometric modeling approach whereby scaled mathematical functions are used to jointly model profile, planform, and cross section aspects of a river valley to create an adjustable model of topography. A key aspect of this framework is the dependent parameterization of channel variability through geomorphic covariance structures (GCSs). A GCS is a spatial covariance series between two or more spatial attributes as a function of position in a river valley. By thinking through how and where geometric variables that control geomorphic process need to covary (or not) it is possible to design a GCS to operationalize a geomorphic process concept via tailored nonuniform, stage-varying channel forms to yield functional form–process dynamics, but this has not been tested yet.

The goal of this study was to demonstrate how GCSs can be generated to create RP topography that either does or does not have flow convergence routing, an explicit form-process linkage thought to maintain undular bed relief and aquatic habitat diversity (MacWilliams et al., 2006). We first develop a GCS associated with RP topography that would experience the flow convergence routing mechanism. Next, we build several synthetic channel models that do and do not have this GCS and then evaluate those channels for the flow convergence routing process. The novelty of this study is that we show how geomorphic theory can be injected into quantitative models of channel topography to yield functional form-process assemblages for scenario analysis in river restoration design.

2. Methods

2.1 Experimental Design

From a single synthetic channel model five different topographic surfaces were created with varying combinations of bankfull width, W_{BF}, and thalweg, Z_T, variability that span the full domain of bed and width undulations and GCS structure. A two dimensional (2D) model was then used in an exploratory mode (sensu Murray, 2007) to simulate a hypothetical high and low discharge in each channel to determine whether any scenario yielded the flow convergence mechanism. Our hypothesis is that based on geomorphic theory (Thompson et al., 1999; MacWilliams et al., 2006; Harrison and Keller, 2007; Caamano et al., 2010; Thompson, 2010) only the surface with positively covarying bed and width undulations that are in-phase should exhibit the test proxies indicative of flow convergence routing discussed below. The presence of flow convergence routing was determined by four tests using the 2D model outputs for shear stress and flow direction. In the first test we qualitatively assessed whether spatially discrete areas of high and low shear stress were created by the topographies at each discharge. For the second test we assessed whether the location of peak shear stress occurred on the riffle (e.g., topographic high, Z_{max}) at low discharge and then on the pool at high discharge (e.g., topographic low, Z_{min}). Third, we assessed whether coherent zones of spatial flow divergence and convergence occurred between the two discharges by analyzing changes in 2D model flow direction. Fourth, we assessed whether convergent flow changed location from the riffle to the pool. These four lines of evidence constitute necessary and sufficient conditions substantiating the claim that a particular GCS exhibits or does not exhibit flow convergence routing. These tests rely on 2D maps of shear stress and flow direction change, but 1D profiles of water surface, bed elevation, dimensionless shear stress, and channel width were also generated to understand how each topographic feature can influence shear stress.

Following the scientific reductionism approach, the experiments were kept relatively simple to demonstrate the effectiveness of synthetic form-process design for the process of flow convergence routing and allow for easy interpretation. While meandering and floodplain topography are optional components to add in using the SRV approach (Brown et al., 2014), straight channels are investigated herein to limit the effect of variable channel sinuosity and subsequent secondary flows to simplify interpretations. Also, bed material is kept uniform throughout the channels. No other processes were investigated herein, though it is likely that they are occurring as well. As the science and technology of synthetic design evaluation improves, testing for more complex channels for many geomorphic processes is anticipated.

Each scenario is meant to encapsulate the iterative adjustment of an initially straight channel into various combinations of Z_T and W_{BF} undulations. Further, each scenario beyond the initial straight channel has conceptual ties to varying types of RP couplet restoration. Scenario 1 is a uniform channel with no variations in Z_T and W_{BF}, analogous to canalized rivers (Figure 1,2A). Scenario 2 has only undulations in W_{BF} to represent local widening associated with riffle restoration where it is expected that sufficient sediment supply exists or is conditionally augmented for riffles and pools to differentiate through time on their own (Figure 1,2B). Scenario 3 has only undulations in Z_T and is comparable to rock-riffle design or spawning-bed infill (Figure 1,2C). Scenario 4 represents the ideal GCS for flow convergence where undulations in both W_{BF} and

Z_T are in phase, creating topographic high points in wider than average areas and low points located in narrower than average areas (Figure 1,2D). Scenario 5 has undulations in W_{BF} and Z_T , but they are out phase (Figure 1,2E), creating topography that is analogous to tributary fan rapids (Kieffer, 1985; O'Connor et al., 1986) or are used to create standing waves and hydraulic jumps in whitewater rodeo parks. For all scenarios we assume Z_{max} and Z_{min} of the bed profile to be the riffle crest and the pool trough, respectively. As such, S1 and S2 do not have bed variations and there are no topographic high or lows to assess. However, S2 can be interpreted in the context of local widening to reduce shear stress (Weber et al., 2009) where the riffle would presumably form in the expansion if adequate flow and sediment supply exist.

2.2 Synthetic testbeds

Digital river testbeds were created using the synthetic river valley (SRV) framework of Brown et al. (2014). Herein we only provide the equations vital to understand the manipulation of SRV channels, while more information can be found in Brown et al. (2014).. The SRV approach creates a reach-averaged equilibrium channel that is scaled by the bankfull width and depth, with the width being an input and the bankfull depth being determined from bankfull width, $\overline{W_{BF}}$ along with the median sediment size, $\overline{D_{50}}$ and slope, $\bar{S}$. Assuming $\overline{H_{BF}}$ is approximated by the hydraulic radius, the reach average bankfull depth, $\overline{H_{BF}}$, was determined by assuming that the depth at incipient motion can be approximated by:

$$\overline{H_{BF}} \sim \overline{H_{critical}} = \frac{(\gamma_S - \gamma_W)\overline{D_{50}}\overline{\tau_c^*}}{\gamma_W \bar{S}} \quad (1)$$

where γ_s and γ_w are the specific weight of sediment and water, respectively. For each channel scenario there were 394 longitudinal nodes spaced at ~ 6 m (1/5 bankfull channel widths) with a total length of 2,364 m. Cross section node spacing was between 2 to 3 m (~1/10 bankfull channel widths). The same input reach-average values were used for each channel scenario where $\overline{W_{BF}}$ = 30 m, $\bar{S}$= 0.002, $\overline{D_{50}}$= 0.32 m, and $\bar{\tau}_c^*$ =0.04, which yielded $\overline{H_{BF}}$ = 2.1 m. Since the channels were straight all equations were in a Cartesian coordinate system.

To understand how sub-reach variability is created in the geometric model it is important to note the equations used, especially for bed elevation and bankfull width. The bed elevation of the channel thalweg was given by:

$$z_T(x_i) = (\overline{H_{BF}}\, f(x_i) + \overline{H_{BF}}) + \bar{S}(\Delta x_i) + Z_D \quad (2)$$

where $Z_D$is a user-defined datum. The top of bank ,Z_{TOB}, was determined by adding the $\overline{H_{BF}}$ to the height of the maximum bed undulation for the detrended thalweg series. The local bankfull width at each location x_i was given by:

$$w_{BF}\,(x_i) = \overline{W_{BF}}\, f(x_i) + \overline{W_{BF}} \quad (3)$$

where $w_{BF}\,(x_i)$ is the local bankfull width at location x_i and $\overline{W_{BF}}$is the reach-average bankfull width. In this study the Deutsch and Wang (1996) cross section model was used for the channel cross sections. Since there was no curvature in the synthetic channels, the cross section geometry was parabolic.

The variability of Z_T and W_{BF} about the reach averaged values was determined by a control function, $f(x_i)$ nested in equations 2 and 3. In this study $f(x_i)$ was modeled using a sinusoid as:

$$y(x_i) = \ a_s\, sin(b_s x_r + \theta_s) \quad (4)$$

where y_i is the dependent control function value, a_s, b_s, and θ_s are the amplitude, angular frequency, and phase for the sinusoidal component, and x_r is the Cartesian stationing in radians. The Cartesian stationing was scaled by $\overline{W_{BF}}$ so that the actual distance was given by $x_i = x_r\overline{W_{BF}}$.

2.3 GCS parameterization

A tremendous amount of research into the maintenance and formation of RP couplets suggests an ideal GCS, where at some channel forming flow the topographic high points have wider flow widths than topographic low points (Keller, 1978; Carling and Wood, 1994; Thompson et al., 1999; Wheaton et al., 2004; MacWilliams et al., 2006; Harrison and Keller, 2007; Caamano et al., 2010; Sawyer et al., 2010; Thompson, 2010; White et al., 2010; Rhoads et al., 2011). Therefore, the GCS needed for RP unit maintenance requires positively covarying bed and bankfull width oscillations. One the basis of 1D analysis there is quantitative guidance on the relative variations of width and depth needed for flow convergence that can be used to further quantify the GCS (Carling and Wood, 1994; Caamano et al., 2009). Using a 1D hydraulic model Carling and Wood (1994) found that they need to be 50% wider than pools or pools need to be rougher than riffles for a reversal in mean velocity. Caamano et al (2009) developed a state space that suggests that both width and depth variations are controls on whether a flow reversal occurs. Specifically, for uniform roughness and assuming equal head losses they show that width variations need to be greater than depth variations for a convergence or reversal. The Caamano relationship is:

$$\frac{W_r}{W_p} = 1 + \frac{h_r}{h_{res}} \quad (5)$$

where h_r is the flow depth over the riffle, h_{res} is the residual pool depth, W_r is the width of the riffle and $W_p$is the width of the pool at the bankfull discharge. For simple case where bed and width undulations are in phase and have the same frequency equations 1–4 can be used to contextualize the SRV model to the Caamano relationship. Based on equations 1–4, h_r is equal to $\overline{H_{BF}}$. The residual pool depth, h_{res}, can be determined as the vertical difference between the maximum and minimum bed undulations (e.g. the riffle crest and pool trough, respectively) and accounting for the fact that the bed is sloped. From equations 2 and 4 the residual pool depth, h_{res}, can be determined as:

$$h_{res} = 2\overline{H_{BF}}a_Z - \pi \frac{\overline{W_{BF}}}{b_Z}\bar{S} \qquad (6)$$

where a_Z is the amplitude of bed undulations and $b_Z$is the angular frequency. Assuming there are no phase shifts the relative widths are given as:

$$W_r = \overline{W_{BF}}(a_w) + \overline{W_{BF}} \qquad (7)$$

$$W_p = \overline{-W_{BF}}(a_w) + \overline{W_{BF}} \qquad (8)$$

Thus, for the value of a_Z chosen for this study, the maximum and minimum values of $w_{BF}(x_i)$ were 37.5 m and 22.5 m, respectively. Combining equations 5-8 yields:

$$\frac{\overline{W_{BF}}(a_w)+\overline{W_{BF}}}{-\overline{W_{BF}}(a_w)+\overline{W_{BF}}} = 1 + \frac{\overline{H_{BF}}}{2\overline{H_{BF}}a_Z - \pi \frac{\overline{W_{BF}}}{b_Z}\bar{S}} \qquad (9)$$

illustrating how one can adjust a terrain with the state space of the Caamano criteria using the reach-averaged input values and a_Z, a_w and b_Z for when the frequency and phase of equation 4 are equal for Z_T and W_{BF}. Given the inputs used in this study (Table 1) for the ideal RP scenario (S4) the riffle was 67% wider than the pool and the bankfull riffle depth was 59% greater than the residual pool depth which meets both the Carling and Orr (1994) and Caamano criterion. It’s important to note that the Caamano relationship cannot account for grain size variations nor predict reversals in peak velocity, but it is still thought to be a meaningful first order assessment of the geometric conditions needed for RP maintenance (Jackson et al., 2015).

Since this study is primarily concerned with the relative variations of local W_{BF} and Z_T, only the amplitude and frequency of Eqn. 4 for these two elements were manipulated for S1 through S4 (Table 1). The exception is S5, in which a phase shift of π was also used in the bed elevation model. In general, b_Z and b_W can be initially specified independently from the literature on RP spacing in alluvial channels or in real world cases from the actual bedform spacing. For each scenario of Z_T and W_{BF} variations had b_Z and b_W equal to 1 (Table 1), yielding a wavelength of 188 m and riffle to pool spacing of 6.28 channel widths. This was chosen to approximate the modal value of pool to riffle spacing reported in the literature (Keller and Melhorn, 1978). Given the model domain length this yielded 13 repeating RP couplets. However, only a central RP couplet was analyzed to avoid potential boundary condition effects in the 2D model.

2.4 2D hydrodynamic modeling

2D modeling was done using Surface Water Modeling System 10.1 for computational mesh preparation and Sedimentation and River Hydraulics- Two-Dimensional (SRH-2D) for solving the depth-averaged St. Venant equations. Model outputs include point based water surface elevation, water depth, depth-averaged velocity components, depth-averaged water speed, Froude number, and shear stress in the direction of flow. For more information, see Lai (2010), Pasternack (2011). A computational mesh for each scenario was constructed with ~ 1 m internodal spacing and sufficient width and elevation to span discharges ranging from 5 to 125 m^3/s. Turbulence closure was achieved with a depth-averaged parabolic turbulence model with an eddy viscosity coefficient of 0.1. This value yields suitable lateral shear zones based on extensive modeling experience for the types of streams investigated herein.

In this study 2D model outputs were used to calculate shear stress components with the following equations:

$$\begin{pmatrix}\tau_{bx}\\ \tau_{by}\end{pmatrix} = \rho C_f \begin{pmatrix}U\\ V\end{pmatrix}\sqrt{(U^2+V^2)} \text{ and } C_f = \frac{gn^2}{h^{1/3}} \qquad (10,11)$$

where τ_{xy} and τ_{by} are the stresses at the bed, ρ is the density of water, C_f is the drag coefficient, n is the Manning coefficient, g is the gravitational constant, h is the flow depth, and U and V are the depth averaged velocity components in the X and Y directions, respectively (Lai, 2010). Pasternack et al. (2006) discuss how 2D model derived shear stresses compare to field derived estimates.

In natural rivers friction is generated by many elements at different spatial scales, including grain roughness, bedforms, channel geometry, and vegetation. Unresolved hydraulic roughness is often quantified using Manning's n value or Darcy-Weisbach friction factor f, which can be spatially variable and stage dependent (Robert, 1990; Lopez and Barragan, 2008). Prior studies using 1D and 2D modeling have shown that roughness differentiation can modulate flow reversals (Carling and Wood, 1994; Jackson et al., 2015). However, in this study only a single value for grain roughness was considered, because we sought to isolate the effects of channel geometry as much as possible from other environmental controls, and synthetic modeling by definition precludes actual empirical calibration that would give such a path merit. To determine the grain roughness the Manning's n value was determined by k_s in its relation to the median grain size by $n = 0.034(k_s)^{1/6}$ and $k_s = 6.1\,D_{50}$ where n = Manning's roughness, k_s = equivalent bed roughness, D_{50} = median bed sediment size (Lopez and Barragan, 2008).

This study involved simulating steady state hydrodynamics over synthetic river topography, so estimated synthetic discharges were needed. To create flows in each test river an area-subdivision method was used on the downstream cross section assuming steady, uniform flow at that location. Each channel scenario was designed to have exactly the same downstream boundary cross section so that flows were the same for all scenarios. For each increment of cross sectional flow area, the Manning and continuity equations were applied:

$$\bar{V} = \frac{k}{n} R^{2/3} S^{1/2} \text{ and } Q = A\bar{V} \quad (12,13)$$

where $\bar{V}$ is the average cross section velocity, k is an empirical constant equal to 1 for metric units, R is hydraulic radius, S is bed slope, and Q is water discharge. Based on this approach, downstream normal depths of ~ 0.6 and 2.6 m were used for the base flow and bankfull discharges, yielding 5 and 125 m^3/s, respectively. The highest discharge was considered a synthetic bankfull flow, as the channels were filled completely, while the lowest discharge corresponded with ~0.04 times bankfull discharge. For the higher discharge this meant that the water just spilled out of the channel with depths on the lateral terraces less than 0.2 m for S5 and less than 0.05 m for all other runs.

2.5 Data Analysis

The four tests required generating 2D maps of shear stress and flow direction change. To better understand why flow convergence routing does and does not occur for the GCSs 1D longitudinal profiles of shear stress and water surface elevation (WSE) were analyzed for scenarios 2-5. Each shear stress profile was also analyzed to determine the magnitude of any longitudinal changes in zones of peak shear stress. Changes as a function of discharge can include expansion, contraction, shifting, and emergence from nonexistence. Although not an explicit test, the values of peak shear stress are also useful to consider relative to the competent particle size that could exist under those stresses. The competent particle size was found by rearranging equation (1) for particle size and using a value of 0.04 for $\overline{\tau}_c^*$ (Parker et al., 2007). Since the competent particle size is proportional to shear stress, separate maps are not shown because the patterns would be identical.

To generate the dataset, ArcGIS was used to process and analyze 2D model outputs. To isolate potential boundary condition effects, results were only analyzed within a 188-m domain of the total model length, starting at station 1043 and ending at station 1271. For each simulation 2D model outputs of point variables were converted into triangular irregular elements (TINs) for visualization in 2D maps. A centerline was generated in ArcGIS and nodes created at 1 m intervals to extract shear stress and WSE at each centerline node.

For flow direction, we assessed changes in direction for each model point relative to the main flow path direction of 180° as in Brown and Pasternack (2014). To do this, the main flow path direction of 180° was subtracted from the Cartesian flow direction of each model node yielding a map of changes in flow direction. To illustrate results 2D maps were made with 8 bin categories were used for positive and negative deviations from the centerline +/- 0-15, 15-45, 45-90, 90-180° . Because changes in flow direction are taken relative to the centerline, values need to be interpreted relative to the side of river (e.g. river right or left) they occur on. For flow cells to the right of the centerline, negative values correspond to flow direction changes in which a flow vector is oriented towards river right, and positive values when a flow vector is oriented towards river left or the centerline. Conversely, for flow cells to the left of the centerline, negative values correspond to flow direction changes in which a flow vector is oriented towards river left, and positive values when a flow vector is oriented towards river right or the centerline. Similarly, negative and positive values greater than 90° correspond to flow vectors that are at the onset of eddying upstream. Note that an eddy would have flow spanning the full domain of flow direction change from 0 to +/-180°. For a convergent jet, it is expected that a narrow band of converging flow will also have adjacent eddies (Thompson et al., 1999). To help interpret the results we focus on three common patterns associated with flow convergence including eddies, laterally convergent flow and laterally divergent flow. In addition to 2D maps of flow direction change, percent rank statistics were calculated for +/- 5, 15 and 45° to determine the overall amount of variability in the flow direction change field.

3. Results

3.1 Test 1: Shear stress patterns

Other than S1, each scenario had a spatially discrete zone of peak shear stress and there were coherent regions of both increases and decreases in shear stress with increasing discharge (Fig. 3,4). In S1 there were no variations in either W_{BF} or Z_T and subsequently there were no variations in the spatial patterns of shear stress at either stage (Fig. 3A,B). The variations of W_{BF} in S2 produced peak values of shear stress that coincided with W_{min} at both stages (Fig. 3C,D, Fig. 4A,B). Qualitatively the patterns remained very similar between the two discharges (Fig. 4A,B). For S3 a peak in shear stress was present near Z_{max} also coinciding with breaks in WSE regardless of discharge (Fig. 4C,D). The shape of the profile was very sharp at the low discharge and became more dampened at the higher discharge (Fig.4 C,D). For S4 the low flow shear stress profile was characterized by a large asymmetrical spike ~ 15 m downstream of Z_{max} that coincided with a break in WSE (Fig.4 E,F). The high flow profile changed completely with two peaks associated with W_{min} and Z_{max} (Fig.4 E,F). Roughly half of the longitudinal profile exhibited an increase in shear stress at the bankfull flow, but more importantly, the other half exhibited a drop in shear stress despite having more flow. The lowest value of shear stress was found not in Z_{max} or Z_{min}, but approximately in between them. For S5 persistent peaks in the spatial pattern of shear stress exist on Z_{max} at all flows (Fig.4 G,H). The low flow shear stress profile has a sharp peak analogous to S3 and S4 while at the higher discharge the total range of the profile contracts and the overall shape changes slightly.

The absolute values of peak shear stress are also useful to consider relative to the competent particle size that could exist under those stresses (Table 4). The maximum value of shear stress occurred in S5, with a value of 74 N/m^2, which yields a competent grain size of 0.115 m. The S5 scenario also had the lowest average shear stress. The lowest values of peak shear stress (and competent grain size) occurred for S1 and S4. The scenario with the closet average competent grain size closest to the reach –averaged value specified in the model setup was S1, which also had the highest average shear stress amongst all scenarios.

3.2 Test 2: Shear stress pattern shift

Scenarios 2 through 5 had spatially discrete peaks in shear stress and only one of these scenarios showed a shift in the location from near Z_{max} to Z_{min} (Fig. 3,4). In S3, S4, and S5 the region of peak shear stress expanded from lowest to highest flow and the magnitude of the highest peak decreased. For S2 and S3, there were minor downstream shifts in peak shear stress of 1% and 5%, respectively, of the total RP wavelength between the two extremal flows (Table 3; Fig. 3). For S4 where W_{BF} and Z_T variations were both present and in phase the location of the coherent region of peak shear stress changed from near Z_{max} to Z_{min} (Fig.3 G,H), shifting 41% of the total RP wavelength (Table 3). In S5 where W_{BF} and Z_T variations were out of phase, spatial patterns in shear stress were controlled by these variations but zones changed very little with stage (Fig.3 I,J). The peak value of shear stress had a phase shift of 9% of the total wavelength, coinciding with Z_{max} and W_{min} (Table 3).

3.3 Test 3: Flow direction change patterns

Because the channels were straight and had modest bed and width amplitudes the overall flow patterns for the scenarios were predominately straight (Table 4). For S1, flow directions were uniformly oriented downstream with no longitudinal differences in flow direction patterns at either discharge (Figure A,B; Table 4). For S2 there was a weak flow divergence near W_{max} and flow convergence near W_{min} at the low discharge, as indicated by checkerboard color patterns in Figure 6C. In contrast, at the higher discharge flow was oriented downstream with no coherent zones of flow convergence or divergence (Fig. 5D). The overall changes flow directions for S2 were mostly straight with 95% and 85% of the data having deviations in flow direction less than 5°, for the low and high flow respectively (Table 4). For S3 at the low discharge there was evidence of convergent flow beginning upstream of Z_{max} that created a narrow jet with two adjacent eddies through Z_{min} (Fig. 5E). At the high discharge the zone of flow convergence shrinks longitudinally as a coherent zone of flow divergence begins just above Z_{min} (Fig. 5F). Compared to S2 and S1, flow directions in S3 were much more variable with at the low discharge, but this variability decreased at the high discharge (Table 4). For S4 at the low discharge flow converges above Z_{max} forming an eddy bounded jet while approaching Z_{min}(Fig. 5GH). At the high discharge similar patterns prevail, but the onset of converging and diverging flow shifts (Fig. 5H). Of all the scenarios S5 had the greatest variation in flow direction change with 22 and 14% of the data having deviations greater than 45° at the low and high discharge, respectively. The flow patterns for the low discharge show flow convergence where Z_{max} and W_{max} coincide (Fig. 5I). Downstream of this area an asymmetrical jet forms in the downstream pool with two eddies on both sides. At the high discharge the jet strengthens and follows the channel walls and the eddies move into the width expansion (e.g. W_{max}) but there is not a clear divergence or convergence of flow directions (Fig. 5J).

3.4 Test 4: Flow direction change pattern shift

The final test determined if any of the topographic surfaces experienced a shift in the location of convergent flow vectors from low to high discharges. Only S3 and S4 are discussed in this section as they both had discrete zones of flow convergence and divergence at both discharges (Figure). At the low discharge both S3 and S4 exhibited convergent flow upstream of Z_{max} that created a narrow jet with two adjacent eddies through Z_{min} (Fig. EG). However, only S4 has a clear pattern of flow divergence following this. While they have similar patterns at the high discharge, the locations of where flow patterns change are also different. For S3, flow convergence begins ~ 12 m upstream of Z_{max} while flow divergence begins ~ 22 m upstream of Z_{min}. Contrasting this for S4, the locations of the onset of converging and diverging flow occur in within 2 m of Z_{max} and Z_{min}, respectively. Thus, only S4 experienced a shift in the location of converging and diverging flow consistent with the theory of flow convergence routing.

4. Discussion

4.1 Process based design of riffle-pool topography

The results above show that only the S4 GCS configuration produces a reach-scale channel morphology that yielded 2D model results consistent with the process of flow convergence routing. Overall, when there was only one level of topographic variability peak zones of shear stress were controlled by Z_{max} or W_{min} irrespective of discharge. To make the locations of peak shear stress change with increasing discharge an additional topographic feature needs to be present that is not collocated with the low flow hydraulic control. For example, both S4 and S5, variations in peak shear stress are driven by Z_{max} at the low discharge and W_{min} at the high discharge. However, a shift only occurs when variations in Z_{max} and W_{min} covary as in S4. Thus, the restoration of RP couplets with the intent of instilling flow convergence routing as the primary mechanism for insuring that RP relief is maintained should use this configuration as a starting point in developing river and stream restoration designs.

This simplification of channel topography as a control on RP maintenance does not disregard the importance of local variability (Harrison and Keller, 2007), substrate (Milne, 1982), sediment supply (Caamano et al., 2010), and turbulence (MacVicar and Best, 2013). Rather, it is a representation of the required geometry needed to create a first order design topography to actively recreate and restore a well-known process through RP couplets in the fluvial landform that practitioners most commonly use. Subsequent flow, sediment, and habitat modeling can be used to drive design iterations, which are easily made through parameter adjustments to the amplitude, phase and frequency of W_{BF} and Z_T in the SRV model used in this paper. Also, even if planners intend to vary the bed material composition between riffles and pools to institute other RP sustainability mechanisms, it would still be wise to enable flow convergence through geometric manipulation facilitated by this GCS method to have multiple supporting processes at work, especially where sediment supply constraints exist. In the future multidimensional morphodynamic models with explicit turbulence may account for all of the existent mechanisms present, but at this time the use of 2D hydrodynamic modeling provides a substantial improvement over current practices that do not involve thorough testing of design alternatives prior to construction. Such 2D modeling can be done quickly and at reasonable cost compared to the total cost of a river project.

It is also worthwhile to consider scenarios 2 and 3 in the context of contemporary RP restoration approaches. A process based approach to restoring river channels is to selectively widen certain areas so that local aggradation may occur where relative stream competence is lower, analogous to S2 (Weber et al., 2009). Our results show that the peak shear stress and velocity would occur in the constriction at all discharges for the fixed bed simulations considered here. However, it is likely that morphodynamic feedbacks would occur wherein the bed aggrades in the width expansion, as the flow is concentrated into an effective-width zone and deposition tends to occur in the peripheral slackwater regions. Such aggradation would raise the bed profile locally and create zones of high velocity and shear stress at low flows (Weber et al., 2009). Thus, even though this GCS does not create conditions associated with flow convergence immediately, over time morphodynamic processes may instill undular relief such as in S4 as long as suitable sediment supply and flow regimes are present.

Contrasting this, S3 had only Z_T undulations and represents a case analogous to the geometry of rock-riffles where only the longitudinal profile is manipulated (Walker et al., 2004; Newbury et al., 2011). This scenario shows that rock-riffle configurations that do not have corresponding width undulations in phase with the channel bed will always be zones of high shear stress regardless of discharge. These types of instream structures may provide an improvement in hydraulic diversity at base flows when compared to canalized rivers, but may be limited in their functionality beyond this and may fall apart over time, necessitating undesirable over-engineering. For example, if these types of features are designed for spawning to occur near the riffle crest then they would likely pose a risk to embryo scour during high flows or would require coarse enough substrate to remain stable across the full flow regime. In cases where immobile material is needed for stability this could have impacts to macro-invertebrate communities that may benefit from some temporal disturbance (Townsend et al., 1997; McCabe and Gotelli, 2000). Further, if stability concerns (Walker et al., 2004) require the emplacement of large substrate to resist scour, then that size could prohibit spawning altogether (Bjorn and Reiser, 1991). Our results suggest that manipulating the channel bed (Walker et al., 2004; Newbury et al., 2011) or width alone will not induce flow convergence, although the latter may develop topography that does over time. Thus, form-process restoration concerned with creating, enhancing or restoring RP couplets should focus on creating channels with both width and bed undulations that are in phase. This however does not preclude the broader needs of a proper flow and sediment regime in managed systems (Kondolf, 2013).

4.2 New insights into flow direction patterns

While many studies conceptually show the lateral funneling of flow as being an important component of the flow convergence routing mechanism (e.g. MacWilliams et al., 2006; Thompson, 2010), few have actually evaluated it quantitatively so it is not possible to compare or contrast these results. However, this does not preclude discussing qualitative observations. Overall, the magnitude of flow variation was relatively low as the channels were designed to be straight (Table 4). Out of all of the scenarios, S5 produced the most variable flow directions (Table 4). At the low discharge S3 through S5 all had spatial patterns of flow direction change associated with eddy bounded and constricted jet flow due to vertical flow convergence over Z_{min} in accordance with prior work. At the higher discharge this flow structure persisted in these three scenarios, but only in S4 did the location move. Therefore, it appears that relative variations in Z_T and W_{BF} can control the presence of jet flow at low flows, but variations in W_{BF} can become more important at higher flows. This is because bed variations exert diminishing controls on velocity and shear stress with increasing discharge as width variations become more important (White et al., 2010; Wilkinson et al., 2004; Brown and Pasternack, 2014).

4.3 Using GCSs for process based river design

The results of this study demonstrate that specific GCS configurations can create channels with specific form-process linkages. This has considerable potential in more broadly impacting the ecohydraulic design of rivers and streams by providing a succinct method for linking hydrodynamic, geomorphic, and ecological processes to the topographies that create them, while also allowing for controlled iteration. To guide the use of this approach we present a flow chart that illustrates the general use of GCSs and geometric modeling for designing channel and floodplain topography with form-process linkages (Figure). To use this approach more generally in process based river design a first step is establishing design criteria that are related to discharge-specific hydrodynamic spatial patterns in the river corridor. This could be to create salmonid habitat units by translating habitat suitability curves to the needed spatial patterns of depth and velocity (Bovee, 1986). This could also be for a wider range of applications outside of river restoration such as designing whitewater steps in river parks. sediment sinks in flood control channels, and channel re-alignments for road and bridge construction. Next, GCS(s) are then developed that would create those spatial patterns and any variability amongst flow discharges. For this study we demonstrated this process by using the theory of flow convergence routing to reverse engineer the topography that would be needed for that process. Once GCS(s) are developed they can be implemented in a geometric model to create design topography. Application to a real world setting would only require specification of the coordinates of the channel centerline and any lateral or vertical limits that may exist in the river corridor. Once design topography is generated it can be evaluated for the original goal(s) and if needed, adjusted and iterated upon further. It is even possible to use this approach in an optimization-simulation context (Maeda, 2013), whereby topographies are iterated to maximize, for example, the amount of spawning habitat created.

The use of control functions within the geometric model allows the designer to rapidly iterate the design topography in lieu of subsequent numerical modeling. While the selection of control functions is ultimately decided by the user, sinusoids allow simple adjustment of the amplitude, frequency and phase of each geometric element. Further, with sinusoids the spectra of real river spatial series could also be used by performing an inverse Fourier transform. A common criticism to using sinusoids is that river bed and width profiles are more variable in nature. However, it’s been demonstrated that sinusoids approximate many channel features, including bed profiles, as a form of minimum variance (Hallet, 1990, Wohl et al., 1999). Further, considering that there can be inherent error in implementing river restoration designs with heavy equipment (Sawyer et al., 2009), this is not considered a problem as sub channel width scale variations can occur through operator error and variations in bed and bank materials. There has been no research on suitable analytical functions for riffle-pool bed topography, or channel width for that matter, and future research may identify better functions. However, for those opposed to sinusoids due to the history of their misuse in river restoration, other functions are available that can be substituted for sinusoids for river synthesis exist, including the more general cnoidal function, a Perlin noise function, and auto-regressive models (Knighton, 1983). Whatever function is used, as long as the synthetic channel design is tested for its form-process mechanisms and found to yield them as predicted, then it is suitable to use them in construction.

While the topographies generated herein may appear simple, they are only meant to be a first order approximation of the reach-scale channel topography that meets to design goals. In actual process-based river design this would be the first topographic surface that would be iterated upon further after subsequent flow, sediment transport, ecologic and morphodynamic modeling. Finer scale variations such as medial bars, boulder clusters, and streamwood can be nested within this overall reach scale template. What makes this approach unique and powerful is that it allows geomorphic theory to be quantitatively injected into the generation and adjustment of river topography. As a result, the GCS approach can unify classification-based and process-based restoration paradigms that have historically been at odds with each other (Small and Doyle, 2012). Classification-based approaches can yield a perceived functional form, which can be synthesized using a single or multiple GCSs that numerical modeling can subsequently evaluate; then modeling can be used to test the design hypothesis assumed in the classification-based approaches to see if they are actually going to be present (e.g., Pasternack and Brown, 2013).

Studies on real RP couplets have shown a great disparity in the discharge that flow convergence routing occurs, ranging from below bankfull (MIlan et al., 2001) to well above bankfull (Sawyer et al., 2010). Managed, altered, and regulated rivers often need to be shifted to entirely new flow regimes. Often, this results in rescaling river corridors such that channel maintenance processes need to now occur at lower discharges (USFWS, 1999). The approach outlined here is thought of as advancement to this problem because it allows one to create and modify the topography needed for flow convergence routing, and the discharge that it occurs. The power of this is that all of the topographic controls on when flow convergence occurs can be altered for specific flow regimes.

4.4 Study limitations and future work

Study limitations include not considering 3D hydraulic patterns, sedimentary and roughness variability, and temporal dynamics ranging from turbulence to morphodynamic feedbacks, all of which have been shown to influence RP sustainability (Milne, 2013; MacVicar and Best, 2013). However, with the exception of sedimentary variability, these are seldom-used controls by practitioners, so this is not seen as a major limitation. Sediment can be accounted for in real-world applications of 2D modeling by plotting Shields stress instead of shear stress (Pasternack, 2011; Jackson et al., 2015). In this study variations in W_{BF} and Z_T were symmetrical due to the use of the sinusoidal control function (Eqn. 8), and it is presumed that they are likely asymmetrical in real rivers. Further while both W_{BF} and Z_T undulations were created to be exactly in phase in this study, empirical evidence suggests that the location of maximum width lags maxima in bed elevations (Richards, 1976; Wilkinson et al., 2004). As shown in Brown et al. (2014), the SRV framework easily allows these manipulations and can rapidly adjust and manipulate the channel topography. This study only looked at one channel slope and different results may arise for steeper slops where the flow approaches critical across a wider domain. While this study primarily focused only on straight channels, meandering rivers are an important planform typology that are commonly restored or rehabilitated and have been shown to exhibit similar phenomena as reported for the straight examples (Brown, 2014). All that is needed to incorporate meandering into these synthetic rivers is to add an additional GCS for bed Z_T and channel curvature as in Brown et al (2014).

Future work should address morphodynamic modeling and effects from changing sediment supply, manipulation of the amplitude of bed and width variations to control the discharge cause specific shifts, exploratory testing of the effects of channel curvature, and using GCSs to analyze real river topography for flow convergence. Given that RP maintenance is a morphodynamic process future work should address evaluating the topographies used in this study with morphodynamic models. Beyond the RP couplet, research should also explore other form-process assemblages that can be used in channel synthesis. Just as GCSs were shown to be valuable in creating channel topography with a specific form-process assemblage they are also useful in assessing rivers for process (Brown and Pasternack, 2014). Future work should also analyze whether the GCS configuration of S4 can be used as a proxy for the occurrence of velocity and shear stress phasing in real rivers.

5. Conclusions

This study illustrated how quantitative models of channel topography can be generated with explicit form-process links by translating conceptual models of RP maintenance to an adjustable quantitative model of channel topography. The basic idea is that if geomorphic, and even ecological, theory can be translated to a GCS then geometric modeling can then be used to generate design surfaces that can be iterated upon further to assess specific ecohydraulic goals and objectives. The use of GCSs in form-process synthesis beyond flow convergence will entail a broader inquiry into whether real rivers have other linkages that can be deduced from coupled spatial series of topography. An Excel© version of the SRV model used to create the scenarios in this study arefreely available at www.rockobrown.com and http://pasternack.ucdavis.edu/.

6. Acknowledgements

The authors would like to acknowledge Jason White for reviewing an early draft of this manuscript, as well as four anonymous reviewers. Financial support was provided by a Henry A. Jastro Graduate Research Award and a research grant from the U. S. Army Corps of Engineers (award # W912HZ-11-2-0038). Funding for G.B. Pasternack was provided by the USDA National Institute of Food and Agriculture, Hatch project number #CA-D-LAW-7034-H.

7. References

Bhowmik N, Adams J, Sparks R (1986) Fate of Navigation Pool on Mississippi River. Journal of Hydraulic Engineering 112: 967–970.

Bjorn TC, Reiser DW (1991) Habitat Requirements of Salmonids in Streams. In: Influences of Forest and Rangeland Management on Salmonid Fishes and Their Habitats. Edited by W.R. Meehan. Special Publication 19. American Fisheries Society. Bethesda, MD. pp. 83-138.

Bovee KD (1986) Development and evaluation of habitat suitability criteria for use in the Instream Flow Incremental Methodology. U.S. Fish Wildlife Service Biologic Report 86(7). 235 pp.

Brown RA (2014) Analysis and synthesis of river topography from geomorphic covariance structures. PhD Dissertation. University of California, Davis.

Brown RA, Pasternack GB, Wallender WW (2014) Synthetic River Valleys: Creating Prescribed Topography for Form-Process Inquiry and River Rehabilitation Design. Geomorphology 214: 40–55.

Brown RA, Pasternack GB (2014) Hydrologic and Topographic Variability Modulates Channel Change in Mountain Rivers. Journal of Hydrology 510: 551–564.

Caamaño D, Goodwin P, Buffington J, Liou J, Daley-Laursen S (2009) Unifying criterion for the velocity reversal hypothesis in gravel-bed rivers. Journal of Hydraulic Engineering 135: 66–70.

Caamaño D, Goodwin P, Buffington JM (2010) Flow structure through pool-riffle sequences and a conceptual model for their sustainability in gravel-bed rivers. River Research and Applications 28: 377–389.

Carling PA, Wood N (1994) Simulation of flow over pool-riffle topography: A consideration of the velocity reversal hypothesis. Earth Surface Processes and Landforms 19: 319–332.

Chang H (1985) Design of Stable Alluvial Canals in a System. Journal of Irrigation Drainage Engineering 111: 36–43.

Chang H, Osmolski Z (1988). Computer-Aided Design for Channelization. Journal of Hydraulic Engineering 114: 1377–1389.Clifford NJ (1993) Differential bed sedimentology and the maintenance of riffle-pool sequences. CATENA 20: 447–468.

Elkins EM, Pasternack GB, Merz JE (2007) Use of slope creation for rehabilitating incised, regulated, gravel bed rivers, Water Resources Research 43, W05432.

Keller EA (1971) Areal Sorting of Bed-Load Material: The Hypothesis of Velocity Reversal. Geological Society of America Bulletin 82: 753-756.

Keller EA (1978) Pools, riffles, and channelization. Environmental Geology 2: 119-127.

Keller EA, Melhorn A (1978) Rhythmic spacing and origin of pools and riffles, Geological Society of America Bulletin 89: 723-730.

Kieffer SW (1985) The 1983 hydraulic jump in Crystal Rapid: Implications for river-running and geomorphic evolution in the Grand Canyon. The Journal of Geology 93: 385-406.

Kim JS, Lee CJ, Kim W, Kim YJ (2010) Roughness coefficient and its uncertainty in gravel-bed rivers. Water Science and Engineering 3: 217-232.

Kondolf GM (2013) Setting Goals in River Restoration: When and Where Can the River "Heal Itself"?. In: Stream Restoration in Dynamic Fluvial Systems. Edited by Simon, A., Bennett, S. J., Castro, J. M., American Geophysical Union, Washington, D. C.

Harrison LR, Keller EA (2007) Modeling forced pool–riffle hydraulics in a boulder-bed stream, southern California. Geomorphology 83: 232–248.

Hallet B (1990) Spatial self-organization in geomorphology: from periodic bedforms and patterned ground to scale-invariant topography, Earth-Science Reviews 29:57–75.

Hodge RA, Sear DA, and Leyland J (2013) Spatial variations in surface sediment structure in riffle-pool sequences: a preliminary test of the Differential Sediment Entrainment Hypothesis. Earth Surface Processes and Landforms 38: 449–465.

Jackson JR, Pasternack GB, and Wheaton JM (2015) Virtual manipulation of topography to test potential pool-riffle maintenance mechanisms. Geomorphology 228: 617–627.

Knighton DM (1983) Models of stream bed topography at the reach scale. Journal of Hydrology 60:105-121.

Lacey G, 1929. Stable channels in alluvium. Proceedings of the Institute of Civil Engineers. London, England, Vol. 229, Part 1, 1930, pp. 259-384.

Lai Y (2010) Two-Dimensional Depth-Averaged Flow Modeling with an Unstructured Hybrid Mesh. Journal of Hydraulic Engineering 136: 12-23.

López R, Barragán J (2008) Equivalent roughness of gravel-bed rivers. Journal of Hydraulic Engineering 134: 847-851.

MacVicar BJ, Best J (2013) A flume experiment on the effect of channel width on the perturbation and recovery of flow in straight pools and riffles with smooth boundaries. Journal of Geophysical Research Earth Surface 118: 1850–1863

MacWilliams ML, Wheaton JM, Pasternack GB, Street RL, Kitanidis PK (2006) Flow convergence routing hypothesis for pool-riffle maintenance in alluvial rivers. Water Resources Research 42, W10427.

Maeda S (2013) A simulation-optimization method for ecohydraulic design of fish habitat in a canal. Ecological Engineering 61:182–189.

Marquis G, Roy A (2011) Bridging the gap between turbulence and larger scales of flow motions in rivers. Earth Surface Processes and Landforms 36: 563–568.

McCabe DJ, Gotelli NJ (2000) Effects of disturbance frequency, intensity, and area on assemblages of stream macroinvertebrates. Oecologia 124: 270-279.

Milan DJ, Heritage GL, Large ARG, Charlton ME (2001) Stage dependent variability in tractive force distribution through a riffle–pool sequence. Catena 44 :85-109.

Milan DJ (2013) Sediment routing hypothesis for pool-riffle maintenance. Earth Surface Processes and Landforms 38: 1623–1641

Milne JA (1982) Bed-material size and the riffle-pool sequence. Sedimentology 29: 267–278.

Murray AB (2007) Reducing model complexity for explanation and prediction. Geomorphology 90: 178–191.

Newbury R, Bates D, and Alex KL (2013) Restoring Habitat Hydraulics with Constructed Riffles, in Stream Restoration in Dynamic Fluvial Systems. Edited by Simon, A., Bennett, S. J., Castro, J. M., American Geophysical Union, Washington, D. C.

Niezgoda S, Johnson P (2005) Improving the Urban Stream Restoration Effort: Identifying Critical Form and Processes Relationships. Environmental Management 5: 579-592.

Parker G, Wilcock PR, Paola C, Dietrich WE, Pitlick J (2007) Physical basis for quasi-universal relations describing bankfull hydraulic geometry of single-thread gravel bed rivers. Journal of Geophysical Research 112 (F4), 1-21.

Pasternack GB (2011) 2D Modeling and Ecohydraulic Analysis. Createspace: Seattle, WA.

Pasternack GB, Wang CL, and Merz J (2004) Application of a 2D hydrodynamic model to reach-scale spawning gravel replenishment on the lower Mokelumne River, California. River Research and Applications 20:2:205-225.

Pasternack GB, Gilbert AT, Wheaton JM, Buckland EM (2006) Error Propagation for Velocity and Shear Stress Prediction Using 2D Models For Environmental Management. Journal of Hydrology 328:227-241

Pasternack GB, Bounrisavong MK, Parikh KK (2008) Backwater control on riffle-pool hydraulics, fish habitat quality, and sediment transport regime in gravel-bed rivers. Journal of Hydrology 357:1-2:125-139.

Pasternack GB (2013) Geomorphologist's Guide to Participating in River Rehabilitation. In: Treatise on Geomorphology. Edited by Shroder, J.F., Wohl, E.E.. Vol 9, Fluvial Geomorphology, San Diego: Academic Press. pp. 843-860.

Pasternack GB, Brown RA (2013) Ecohydraulic Design of Riffle-Pool Relief and Morphological-Unit Geometry in Support of Regulated Gravel-Bed River Rehabilitation. In: Ecohydraulics: an integrated approach. Edited by Maddock, I., Harby, A., Kemp, P., Wood, P. John Wiley & Sons, Ltd. Chichester, UK., pp. 337-355.

Rhoads BL, Engel FL, Abad JD (2013) Pool-Riffle Design Based on Geomorphological Principles for Naturalizing Straight Channels, in Stream Restoration in Dynamic Fluvial Systems. Edited by Simon, A., Bennett, S. J., Castro, J. M., American Geophysical Union, Washington, D. C.

Richards KS (1976) The morphology of riffle-pool sequences. Earth Surface Processes 1:71-88.

Robert A (1990) Boundary roughness in coarse-grained channels. Progress in Physical Geography 14: 42-70.

Sawyer AM, Pasternack GB, Merz JE, Escobar M, Senter AE (2009) Construction constraints on geomorphic-unit rehabilitation on regulated gravel-bed rivers. River Research and Applications 25:416-437.

Sawyer AM, Pasternack GB, Moir HJ, Fulton AA (2010) Riffle-pool maintenance and flow convergence routing confirmed on a large gravel bed river. Geomorphology 114: 143-160.

Schwartz JS, Neff KJ, Dworak FJ, Woockman RR (2014) Restoring riffle-pool structure in an incised, straightened urban stream channel using an ecohydraulic modeling approach. Ecological Engineering. Available online 8 July 2014.

Sear DA (1994) River restoration and geomorphology. Aquatic Conservation: Marine and Freshwater Ecosystems 4: 169–177.

Small MJ, Doyle MW (2011) Historical perspectives on river restoration design in the USA. Progress in Physical Geography 36: 138-153.

Thompson DM (2004) The influence of pool length on local turbulence production and energy slope: a flume experiment. Earth Surf. Process. Landforms, 29: 1341–1358.

Thompson DM (2007) The characteristics of turbulence in a shear zone downstream of a channel constriction in a coarse-grained forced pool. Geomorphology 83:199-214.

Thompson DM (2010) The velocity-reversal hypothesis revisited. Progress in Physical Geography 35: 123-132.

Thompson DM, Wohl EE, Jarrett RD (1999) Velocity reversals and sediment sorting in pools and riffles controlled by channel constrictions. Geomorphology 27: 229–241.

Townsend CR, Scarsbrook MR, Dolédec S (1997) The intermediate disturbance hypothesis, refugia, and biodiversity in streams. Limnological Oceanography 42:938-949.

United States Fish and Wildlife Service (1999) Trinity River Flow Evaluation Report.

Walker DR, Millar RG, Newbury RW (2004) Hydraulic design of riffles in gravel-cobble bed Rivers. International Journal of River Basin Management 2 :291-299.

Weber C, Schager E, Peter A (2009) Habitat diversity and fish assemblage structure in local river widenings: A case study on a Swiss river. River Research Applications, 25: 687–701.

Wheaton J, Pasternack G, Merz J (2004) Spawning habitat rehabilitation - II. Using hypothesis development and testing in design, Mokelumne river, California, U.S.A. International Journal of River Basin Management 2: 21-37.

White JQ, Pasternack GB, Moir HJ (2010) Valley width variation influences riffle-pool location and persistence on a rapidly incising gravel-bed river. Geomorphology 121: 206-221.

Wilkinson SN, Keller RJ, Rutherfurd ID (2004) Phase-shifts in shear stress as an explanation for the maintenance of pool–riffle sequences. Earth Surface Processes and Landforms 29: 737–753.

Wohl E, Thompson DM, Miller AJ (1999) Canyons with undulating walls. Geological Society of America Bulletin 111: 949-959.

8. List of Figures

Figure 1. Synthetic test beds and dimensionless bed and width profiles for the synthetic test beds analyzed in this study. All scenarios have the same slope of 0.002. S1 (A,B) has no bed or width undulations, S2 (B,C) has only width undulations, S3 (D,E) has only bed undulations, S4 (F,G) has bed and width undulations that covary in phase and S5 (H,I) has bed and width undulations that also covary but are out of phase.

Figure 2. Oblique aerial images of real world examples for the five GCS configurations. A prototype for S1 is the urban flood control channel with no bed or bank variations in Los Angeles River, CA (A). An example of local widening comes from a restored reach of Napa River, CA with variations meant to promote riffle restoration (B) analogous with S2. For S3 a prototype is the Lewiston Hatchery Reach of the Trinity River where rock riffles were built in the 1970's to attenuate erosion of spawning gravels (S3). As an example for S4 (D) is a RP unit of the lower Yuba River, CA that appears as a shallow, narrow riffle at low flow (as shown in photo), but at formative discharges (not shown, but its wetted boundary is illustrated as a dashed line) it has a narrow pool (-W,+Z) that transitions into a wide riffle (+W,+Z). Upstream on the same river there is an example of

out-of-phase bed and width undulations analogous to S5 where a narrow step (-W, +Z) occurs just below a wide pool (+W,-Z), and this width difference persists for both base flow (as shown in photo) and formative discharges (not shown, but its wetted boundary is illustrated as a dashed line).

Figure 3. 2D plots of shear stress for the low (left maps) and high discharges (right maps) for S1 (A,B), S2 (C,D), S3 (E,F), S4 (G,H) , and S5 (I,J). The white stars denote topographic high points, Z_{max}, and the white octagons denote topographic low points, Z_{min}, in the bed profile.

Figure 4. Profile plot of water surface elevation, shear stress, bed elevation and relative bankfull width for S2 (A,B), S3 (C,D), S4 (E,F), and S5 (G,H). The black line in the top plot is the bed elevation and the dashed line is the standardized channel width.

Figure 5. 2D plots of flow direction for the low and high discharges for S1 (A,B), S2 (C,D), S3 (E,F), S4 (G,H) , and S5 (I,J). The black stars denote topographic high points, Z_{max}, and the black octagons denote topographic low points, Z_{min}, in the bed profile.

Figure 6. General steps for building GCSs with form-process linkages in river engineering and stream restoration.

Table 1. Width and bed elevation amplitude, frequency and phase for each model scenario.

	Bankfull Width Variation			Bed Variation		
Scenario	Amplitude	Frequency	Phase	Amplitude	Frequency	Phase
S1	0	1	0	0	1	0
S2	0.25	1	0	0	1	0
S3	0	1	0	0.25	1	0
S4	0.25	1	0	0.25	1	0
S5	0.25	1	0	0.25	1	π

Table 2. Relationship between shear stress and competent sediment grain size.

	Shear Stress (N/m2)			Competent grain size (m)		
	Maximum	Average	Standard Deviation	Maximum	Average	Standard Deviation
S1	47	32	13	0.073	0.050	0.018
S2	64	25	18	0.098	0.039	0.025
S3	72	28	20	0.111	0.043	0.028
S4	54	25	18	0.084	0.038	0.028
S5	74	22	20	0.115	0.035	0.028

Table 3. Shifts of maximum shear stress for each scenario with percent of total RP wavelength.

	S1	S2	S3	S4	S5
Shift in maximum (m)	NA	2	10	78	5
Percent of total wavelength	NA	1%	5%	41%	3%

Table 4. Percent rank of flow direction changes for a single wavelength of the 2D model.

	S1		S2		S3		S4		S5	
Value	5	125	5	125	5	125	5	125	5	125
45	100%	100%	100%	99%	77%	90%	90%	95%	78%	86%
15	100%	100%	99%	97%	74%	89%	89%	89%	67%	76%
5	100%	100%	95%	85%	65%	85%	83%	75%	43%	59%

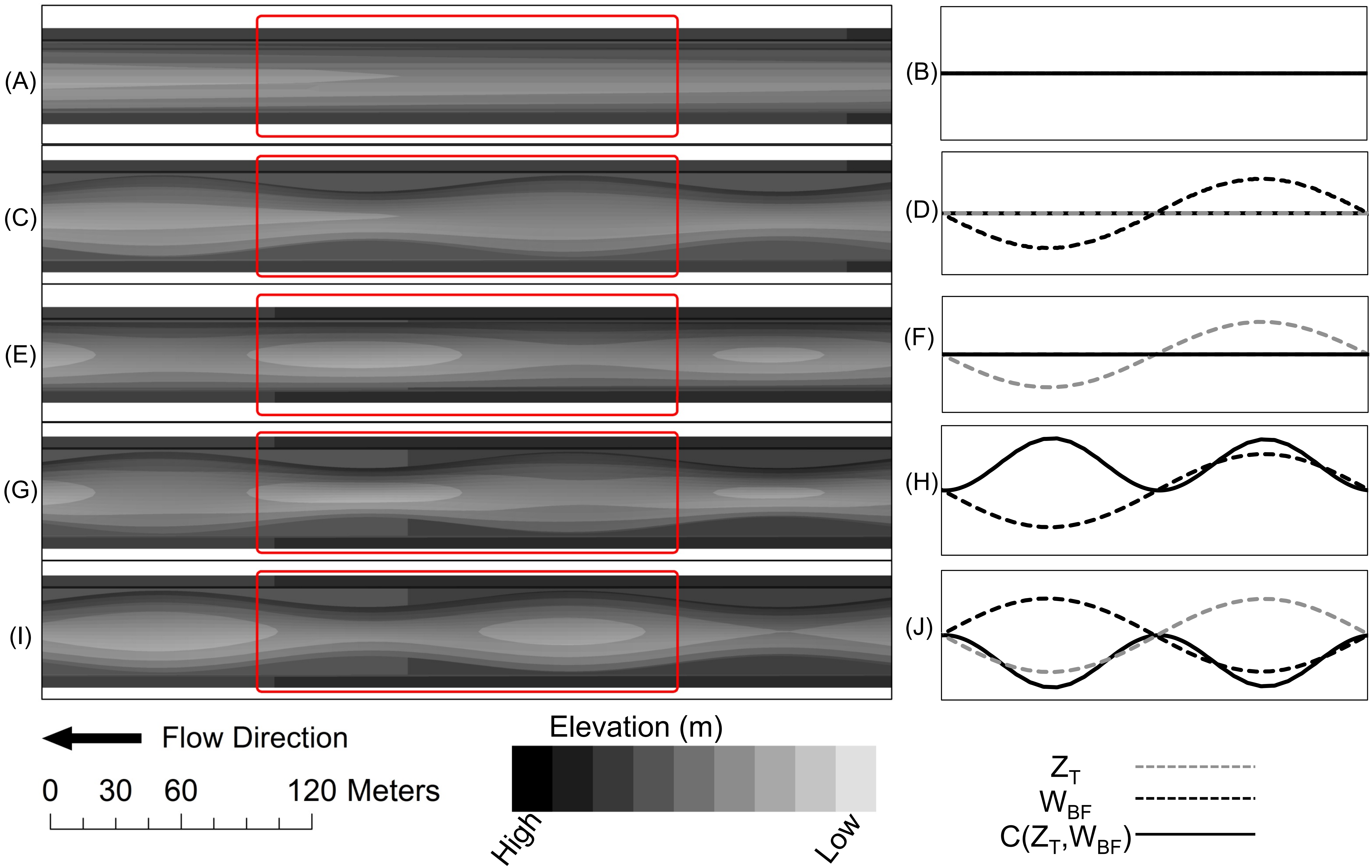

(A)
(B)
(C)
(D)
(E)
(F)
(G)
(H)
(I)
(J)
Flow Direction
0 30 60 120 Meters
Elevation (m)
High
Low
Z_T
W_{BF}
$C(Z_T,W_{BF})$


Flood control channel
Local widening
Rock riffles
Pool
Riffle
Pool
Rapid

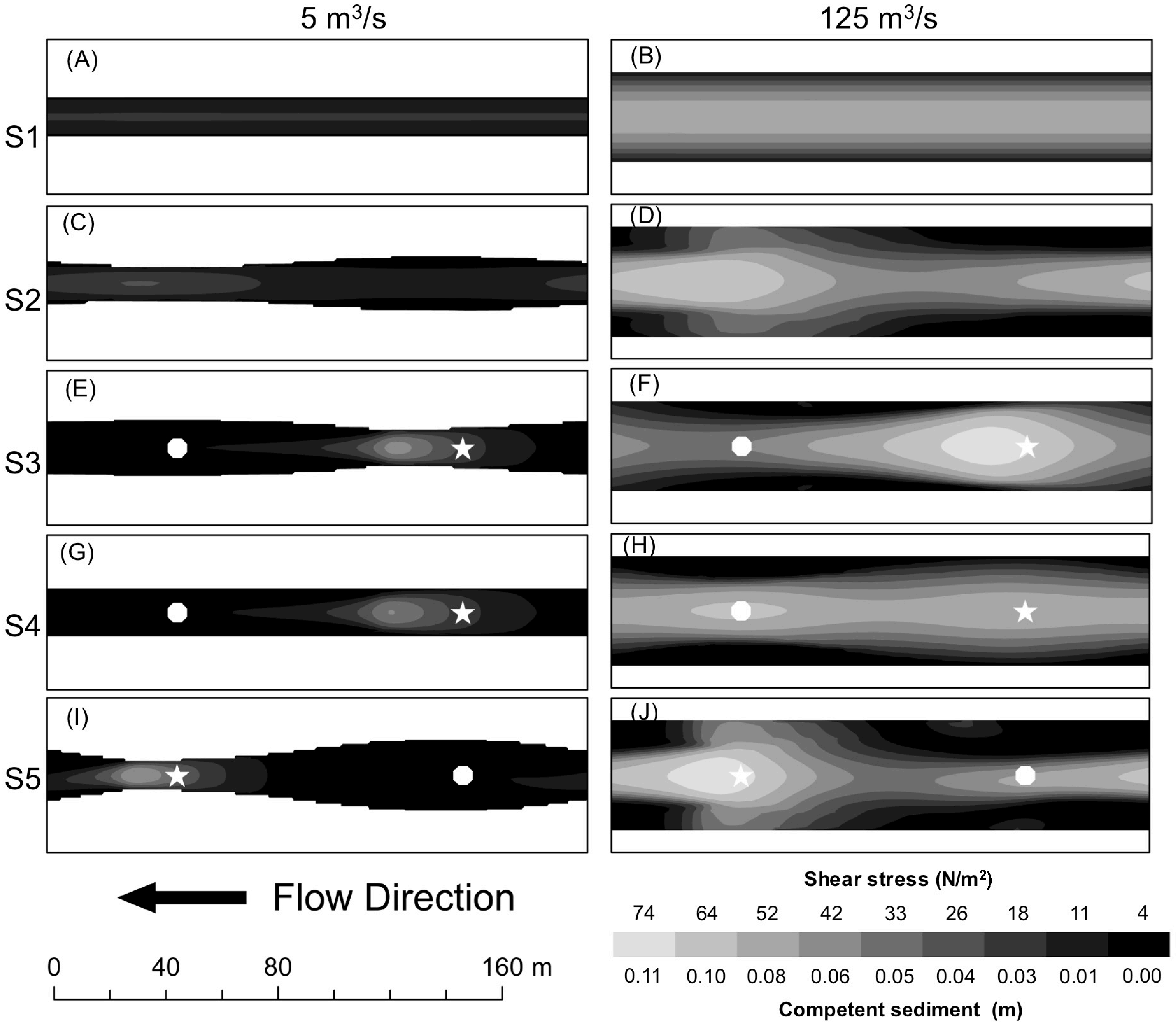
5 m3/s
125 m3/s
(A)
(B)
(C)
(D)
(E)
(F)
(G)
(H)
(I)
(J)
S1
S2
S3
S4
S5
Flow Direction
0
40
80
160 m
Shear stress (N/m2)
74
64
52
42
33
26
18
11
4
0.11
0.10
0.08
0.06
0.05
0.04
0.03
0.01
0.00
Competent sediment (m)

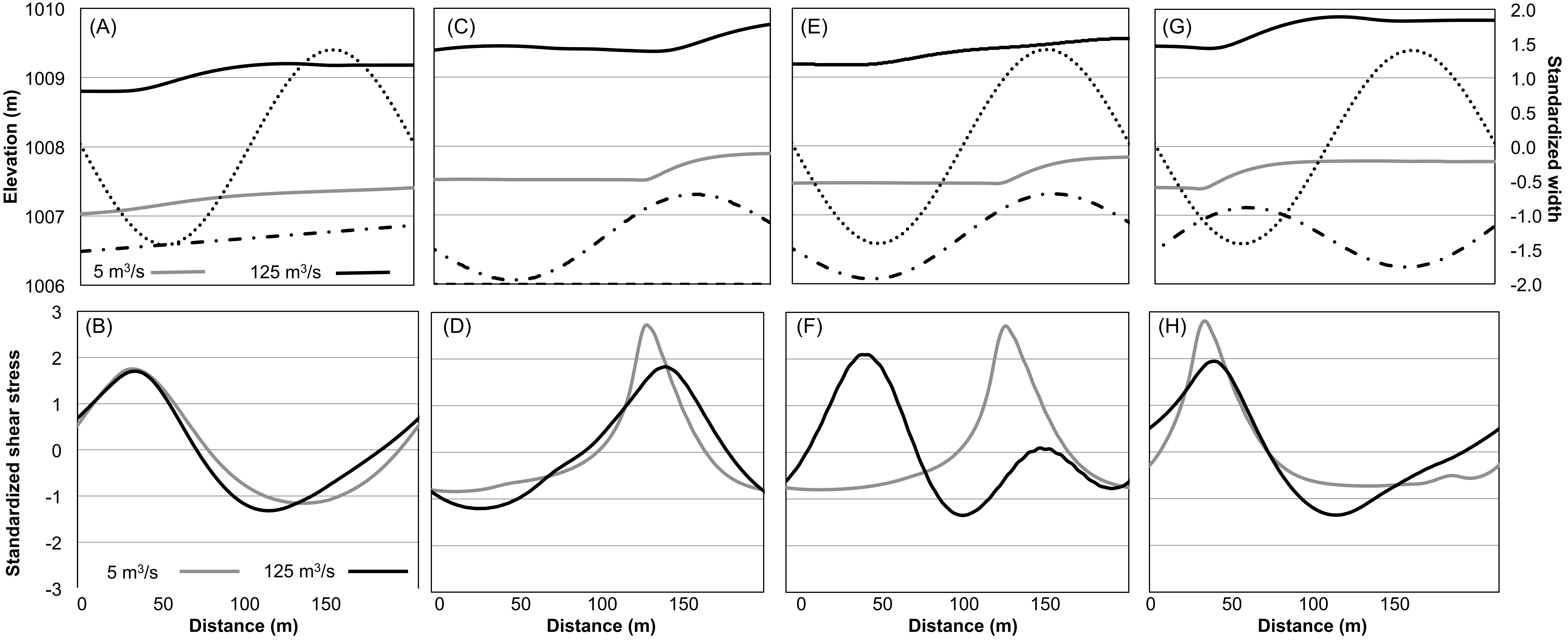

Elevation (m)
Standardized width
Standardized shear stress
(A)
(B)
(C)
(D)
(E)
(F)
(G)
(H)
5 m³/s
125 m³/s
Distance (m)

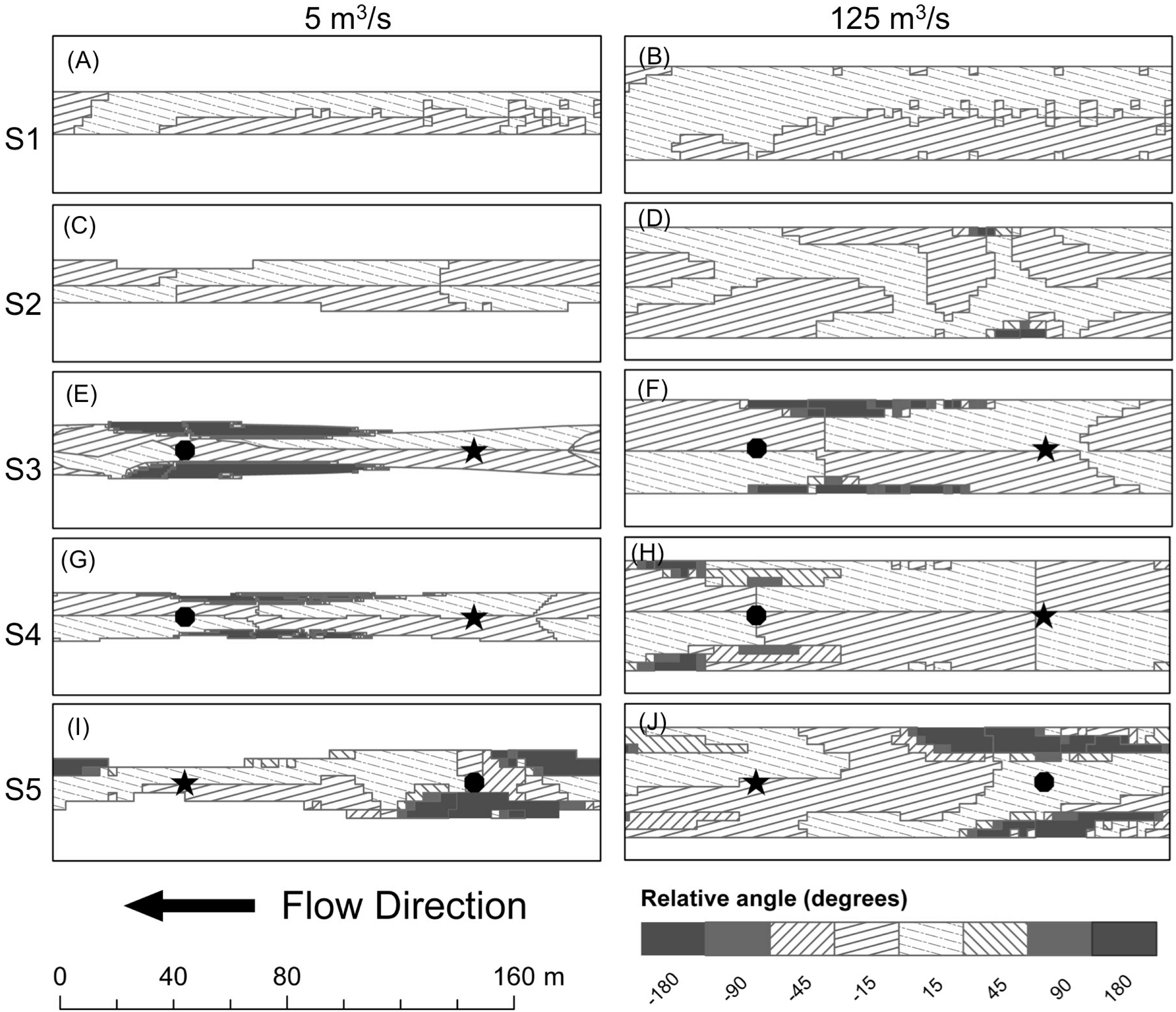
5 m3/s
125 m3/s
(A)
(B)
(C)
(D)
(E)
(F)
(G)
(H)
(I)
(J)
S1
S2
S3
S4
S5
Flow Direction
0
40
80
160 m
Relative angle (degrees)
-180
-90
-45
-15
15
45
90
180

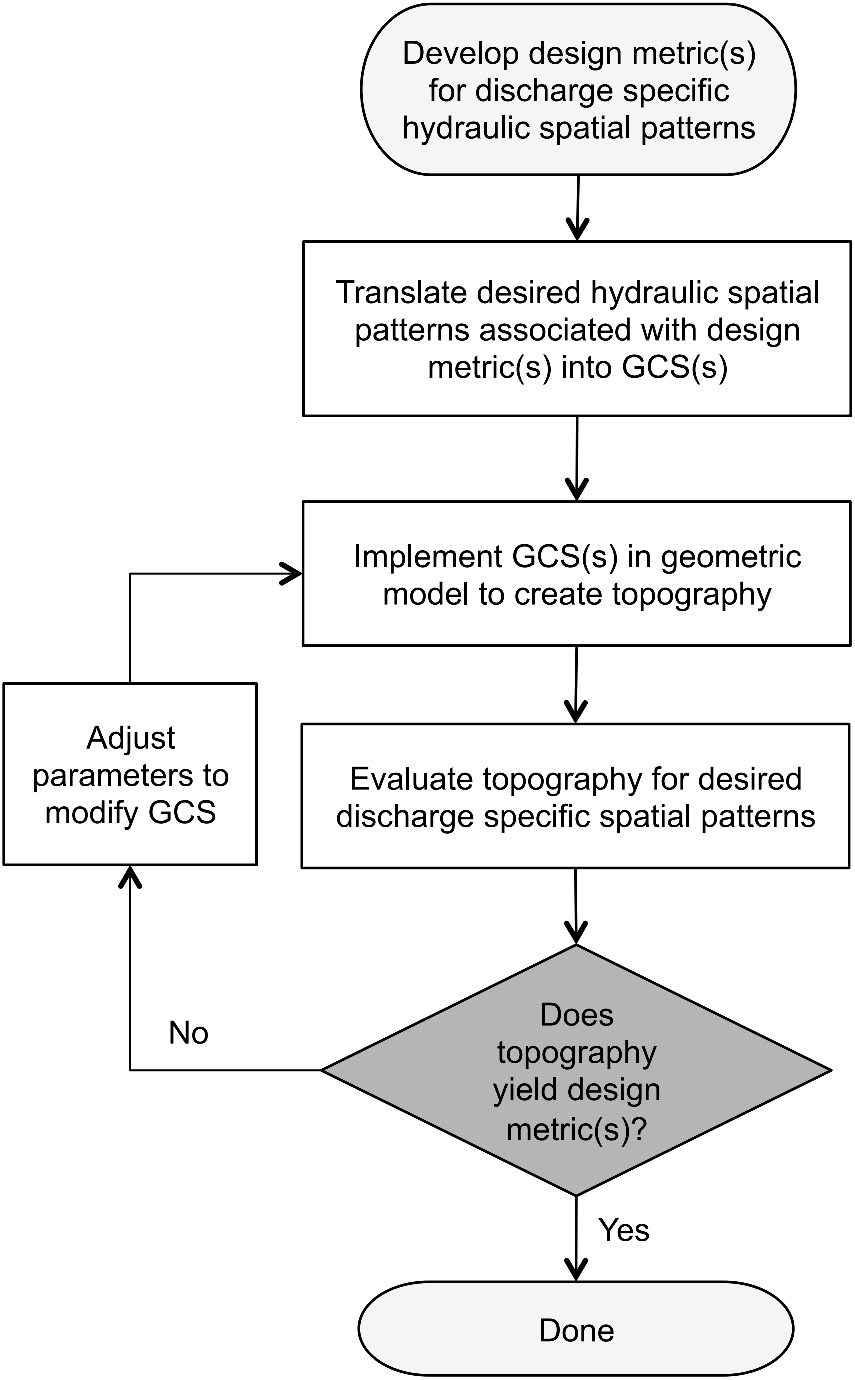
Develop design metric(s) for discharge specific hydraulic spatial patterns
Translate desired hydraulic spatial patterns associated with design metric(s) into GCS(s)
Implement GCS(s) in geometric model to create topography
Evaluate topography for desired discharge specific spatial patterns
Does topography yield design metric(s)?
No
Adjust parameters to modify GCS
Yes
Done